Journal of Power Sources 615 (2024) 235049

Contents lists available at ScienceDirect

Journal of Power Sources

journal homepage: www.elsevier.com/locate/jpowsour

Open source online electrochemical impedance spectroscopy data analytics tool

Alexander Blömeke [a,b,c,*], Ole Kappelhoff [a,b], David Wasylowski [a,b,c], Florian Ringbeck [a,b,c], Dirk Uwe Sauer [a,b,c,d]

[a] Chair for Electrochemical Energy Conversion and Storage Systems (ESS) - Institute for Power Electronics and Electrical Drives (ISEA) - RWTH Aachen University, Campus-Boulevard 89, Aachen, 52074, Germany
[b] Center for Ageing, Reliability and Lifetime Prediction of Electrochemical and Power Electronic Systems (CARL), Germany
[c] Jülich Aachen Research Alliance - JARA-Energy, Germany
[d] IEK-12 - Helmholtz Institute Münster (HI MS) - Forschungszentrum Jülich, Germany

HIGHLIGHTS

- Open Source Tool for Automated Electrochemical Impedance Spectroscopy Analysis.
- Simplification of the Aggregation of Impedance Data from Different Sources.
- Precise Impedance-based Battery Temperature Estimation using SVR.

GRAPHICAL ABSTRACT

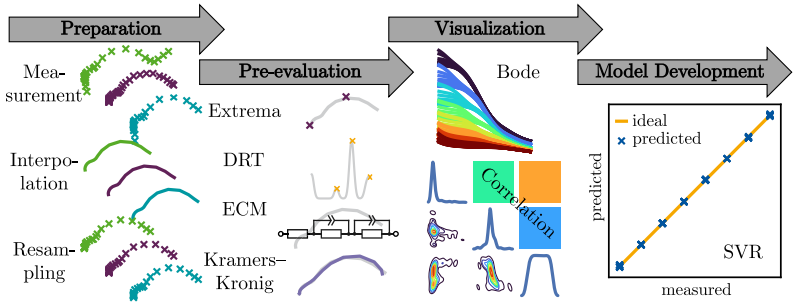

ARTICLE INFO

Dataset link: EIS Data Analytics (Original data) , EIS Data Analytics (Original data)

MSC:
46N30
42-06

Keywords:
Open source
Battery
Electrochemical impedance spectroscopy
Temperature estimation
State-of-X (SOX) estimation

ABSTRACT

This paper presents an open-source platform for automating the analysis of electrochemical impedance spectroscopy measurements to improve energy systems' diagnostic and prognostic capabilities. The platform addresses the main challenges associated with impedance-based estimation techniques in electrochemical energy storage systems, mainly by simplifying the aggregation of impedance data from different sources and enabling the comprehensive application of advanced analytical methods. Initial results, particularly in the area of battery temperature estimation using support vector regression, underline the potential of the tool to improve diagnostic performance. The platform encourages collaborative development, facilitates ongoing improvements, and ensures seamless integration with battery management systems to increase safety and operational efficiency by making it available as open-source software.

* Corresponding author at: Chair for Electrochemical Energy Conversion and Storage Systems (ESS) - Institute for Power Electronics and Electrical Drives (ISEA) - RWTH Aachen University, Campus-Boulevard 89, Aachen, 52074, Germany.
E-mail addresses: alexander.bloemeke@rwth-aachen.de (A. Blömeke), batteries@isea.rwth-aachen.de (D.U. Sauer).

https://doi.org/10.1016/j.jpowsour.2024.235049
Received 12 May 2024; Received in revised form 24 June 2024; Accepted 10 July 2024
Available online 22 July 2024
0378-7753/© 2024 The Author(s). Published by Elsevier B.V. This is an open access article under the CC BY license (http://creativecommons.org/licenses/by/4.0/).

1. Introduction

Impedance spectroscopy is used in many applications to characterize and track the performance of systems [1] or living beings [2]. Fuel cells and batteries are only two examples of electrochemical storage systems that can store energy over long or short periods. The impedance of batteries, without restriction to this energy storage type, varies significantly at different internal or external conditions. As the electrochemical impedance spectroscopy measurements correlate with, for example, temperature, it is interesting to see if such correlations can be translated to a mapping and whether the map is bijective or not. Also, if the electrochemical impedance spectroscopy measurement mapping is bijective for one type of a system, it has to be analyzed if this holds for different system types as well.

For batteries, the electrochemical impedance spectroscopy tracks various changes [3]. For battery cold cranking, the impedance is essential to estimate the state-of-power [4]. Temperature and state-of-charge show great impact on the impedance [5]. Also, aging changes the impedance of batteries [6,7]. Furthermore, critical battery states, like an imminent thermal runaway [8], or lithium-plating due to fast charging [9] can be detected. The battery's performance can be optimized by external pressure, which correlates with the impedance as well [10,11]. But also during battery production, electrochemical impedance spectroscopy is used [12].

The impedance change can be traced back to the change in the characteristics of an individual or many components of the battery. For example, in the literature, the change of impedance caused by aging is linked with solid electrolyte interphase layer growth, loss of active material or loss of lithium inventory, electrolyte and binder decomposition, and others [13–15]. In this publication, no physical–chemical relationships between changing parameters and the impedance are derived. Instead, we refer to existing literature reviews like [16–18]. The focus here is on the generic processing methods for impedance data. The tool presented is not limited to battery data.

Fig. 1 gives an overview of different methods of electrochemical impedance spectroscopy data interpretation. Known from other impedance spectroscopy applications is the analysis of the impedance in the frequency domain, found in the left bottom corner of the triangle. The equivalent circuit models are popular in the field of batteries, which can consist of simple inductors (Ls), resistors (Rs), and capacitors (Cs) or even more complex elements like constant phase elements (CPEs), resistor parallel to a constant phase elements (ZARCs) or Warburg Elements. The distribution of relaxation times maps electrochemical impedance spectroscopy data to a distribution of time constants. The mentioned distribution of relaxation times methods are based on different system assumptions and use different model conceptions. Also, physico-chemical models can be used for explaining electrochemical impedance spectroscopy results. Data-driven approaches vary from regression methods to other machine learning models like neural networks. Computer vision and image processing could interpret figures of electrochemical impedance spectroscopy data. The here presented tool focuses on equivalent circuit models, distribution of relaxation times, and regression methods.

This publication presents the general capabilities of the developed tool using an example data set and an example use case. Firstly, the data used is briefly introduced. The individual processing steps are then presented and discussed in detail. The example case is to estimate the temperature of a battery based on electrochemical impedance spectroscopy measurements at varying state-of-charges. All the results shown here result from this tool, and the processing steps presented.

The example data are measurements performed on LiFun 575166-01 battery cells. The LiFun 575166-01 cells have a 1 Ah nominal capacity, an NMC532 cathode, and a graphite anode. Details about the tests performed are in the supplementary materials [19]. The battery cell choice was driven by project partners, who investigated the cell by nonlinear electrochemical impedance spectroscopy, also known as nonlinear frequency response analysis. A well-known reference chemistry and a lower-capacity battery is favorable for these newer techniques. The cell chemistry or format has no impact on the here presented tool. Other data that has not yet been published or is confidential was also successfully used. In the discussion in the Section 4.1, another chemistry, format, and estimation parameter is used to validate the tool's flexibility.

The impact of state-of-charge and temperature on the impedance of the example battery is shown in Fig. 2. The temperature varies from −15 °C to 55 °C in 10 Kelvin (K) steps, namely −15, −5, 5, 15, 25, 35, 45 and 55 °C. From 0% to 100% the state-of-charge is set in irregular steps to 0, 1, 5, 10,20, 30, 40, 50, 60, 70, 80, 90, 95, 99 and 100% before the measurement. Fig. 2(a) and (c) show the absolute value of the same data. Untypically, for battery measurements, the y-axes of the Bode-diagrams are scaled logarithmically for the absolute values. The phase of the complex impedance is given in Fig. 2(b) and (d). The impact of temperature dominates the impedance curves.

The automated analysis of electrochemical impedance spectroscopy data is necessary to develop methods for evaluation or model development requiring large amounts of data. Different to other tools as presented in [20–24], or [25], the focus of the here developed tool is much more on the harmonization of input data and then the generalization of models. Unifying the frequency points of electrochemical impedance spectroscopy measurements enables the usage of data from various laboratories and equipment. The work of Murbach et al. (2020) [23] and Liu and Ciucci (2020) [24] are embedded into the here presented tool [19].

An important analysis method for deriving battery states and parameters from impedance data is the distribution of relaxation times. The toolchain presented in this article implements this feature by integrating the tool of Liu and Ciucci (2020) [24]. Fig. 3 shows the same data as in Fig. 2, processed by the distribution of relaxation times and, therefore, plotted as a distribution of time constants. Fig. 3 shows that a temperature change causes the impedance's amplitude to change and the time constants identified by the distribution of relaxation times. This indicates that selecting individual frequencies for analyzing the impedance is inadequate for tracking, such as the change of state-of-charge and temperature. Furthermore, it can be seen that a temperature change leads to significant changes in the impedance. A change of the state-of-charge shows a smaller impact.

Over the years, significant progress has been made in battery temperature, state-of-charge, and aging estimation using the impedance. Schmidt et al. (2013) [5] focused on the temperature measurement at varying state-of-charge between 10% and 90% and forced external temperature gradients. Subsequently, Richardson et al. (2014) [26] combined impedance spectroscopy evaluation at 215 Hz with thermal modeling to obtain more accurate estimates of internal temperature. Beelen et al. (2016) [27] then focused on four state-of-charges on the temperature estimation and the sensitivity of different frequencies. The online impedance calculation and temperature estimation, for example, by Wang et al. (2019) [28], investigates the impact of rest time and charge or discharge superposition. The cell and method used by Wang et al. (2020) [29] suggest using the phase of the impedance in the range of 10 Hz to 100 Hz for temperature estimation. Machine learning is used, for example, by Gasper et al. (2022) [21], who investigated the relationship between impedance and capacity at various state-of-charges. Mc Carthy et al. (2022) [30] focused on the use of the imaginary part of the impedance at 200 Hz for temperature estimation. The results by Faraji-Niri et al. (2023) [31] on their dataset from Rashid et al. (2023) [32] for state-of-health estimation will be discussed again in Section 4.1. Recently, the results of Ezahedi et al. (2024) [33] using Gaussian process regression for temperature estimation and those of Liu et al. (2024) [34] for machine-learning-based temperature estimation of sodium-ion batteries have been published. All publications achieve

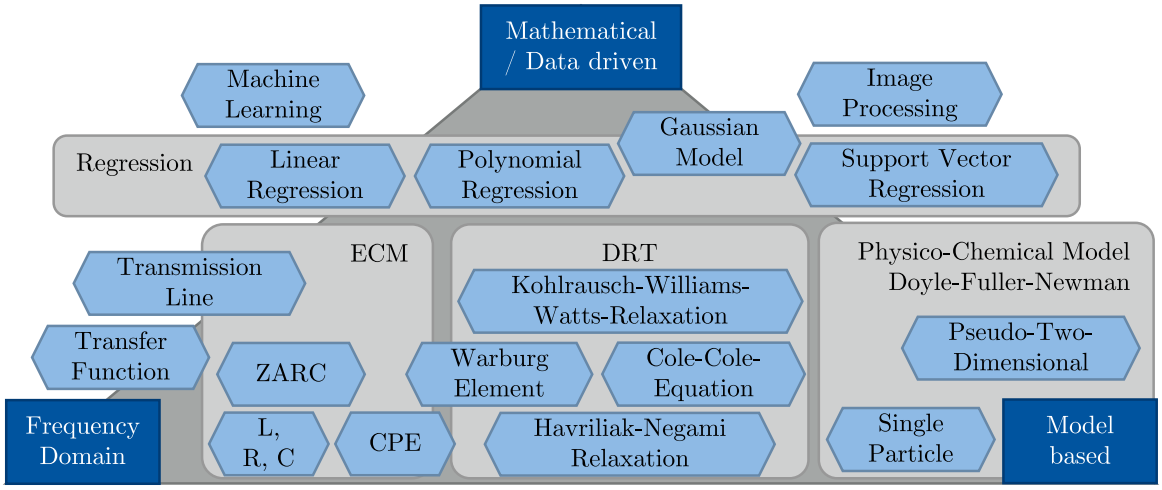

Fig. 1. Overview of different methods of electrochemical impedance spectroscopy (EIS) data interpretation. From methods in the frequency domain (bottom left) over model-based fitting or simulation approaches (bottom right) to purely data-driven concepts.

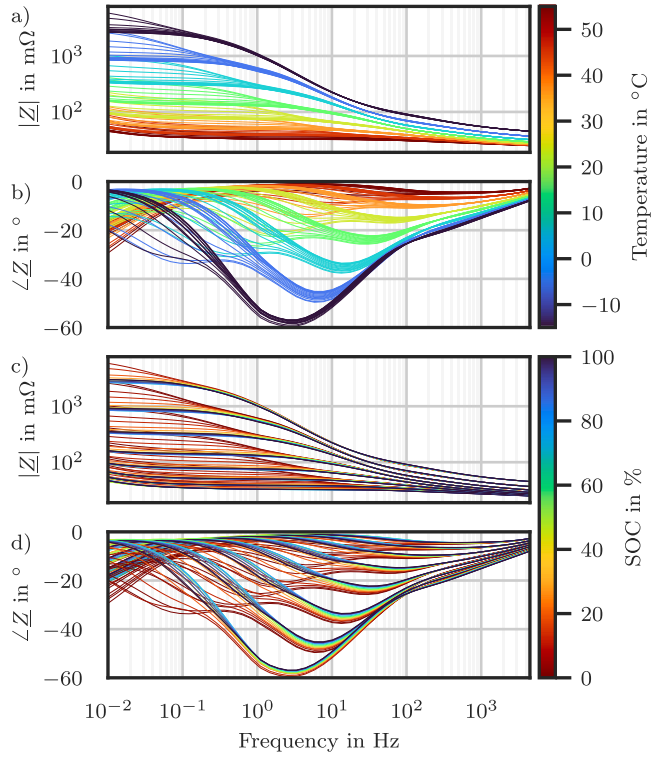

Fig. 2. Dependency of battery electrochemical impedance spectroscopy (EIS) measurements on temperature and state-of-charge (SOC). All plots show the same impedance data. (a) and (c) showing the absolute value with a logarithmic scale. (b) and (d) the phase of the impedance. (a) and (b) are colored according to the temperature of the measurement. The color of the lines of (c) and (d) is selected based on the SOC. (For interpretation of the references to color in this figure legend, the reader is referred to the web version of this article.)

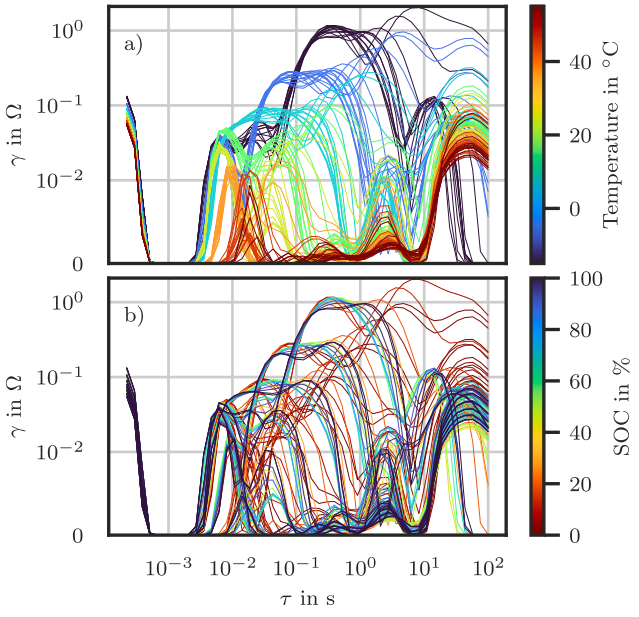

Fig. 3. Dependency of battery distribution of relaxation times (DRT) measurements on temperature and state-of-charge (SOC). All plots use the same impedance data. Extrema are highlighted with marks. (a) is colored according to the temperature of the measurement. The color of the lines of (b) is selected based on the SOC. (For interpretation of the references to color in this figure legend, the reader is referred to the web version of this article.)

root-mean-square-error for the temperature estimation in the range of a few Kelvins.

This publication's most significant impact is its open-source character and reproducibility. All publications and available tools focus on specific uniform impedance data. The harmonization of impedance data and the formatting for further general use is not sufficiently addressed. To verify the flexibility of this tool, the results of [31] are reproduced. The results are briefly discussed in Section 4.1. More details can be found in the repository at: https://git.rwth-aachen.de/isea/eis_data_analytics.

2. Methods

Several approaches exist to obtain information from measurements from electrochemical impedance spectroscopy. Visual representations such as Nyquist or Bode diagrams are helpful for intuitive analysis. If a large amount of data must be analyzed, or if a machine must interpret measurements and respond to a change in impedance, then electrochemical impedance spectroscopy data must be processed automatically. Visual representation for machines, such as with computer vision, would incur significant expense. There are no general

limitations on selecting algorithms for electrochemical impedance spectroscopy data processing. The techniques must be flexible to all conceivable changes in impedance data, such as those produced by variations in the temperature of the tested battery.

As long as the number of changing parameters of the device under test is limited and the associated impedance changes are bounded, most methods may be optimized to decrease the root-mean-square error between fitted data and original data. If the device under test is a battery whose impedance is affected by factors such as temperature, state-of-charge, state-of-health, pressure, and many more, this might lead to high-dimensional fitting issues, which are often not bijective [5]. The error may be reduced when the order of the underlying mathematical description approach, such as equivalent circuit models, increases. If the increased order results in an overdetermined system, then the system's parameters become arbitrary. Arbitrary parameters cannot be automatically evaluated since their association to, say, a change in temperature is no longer specified. Often, the order of parameters or a group of parameters must be minimized to achieve their uniqueness.

Other aspects are the generalization, interpolation, and extrapolation of models. Methods not based on sufficiently validated physical or chemical assumptions can rarely be used for extrapolation. Interpolation can compensate for a lack of system understanding by using many measurements. Generalizability without the use of physical–chemical relations depends strongly on the data used. The example presented here in the paper is only tested for interpolatability.

This publication aims to present the developed tool without focusing too much on a specific application. To describe the tool based on an example, the temperature of various state-of-charges is estimated in the following using support vector machine regression with an radial basis function kernel.

3. Results

The here developed *EIS Data Analytics* [19] tool is designed to convert measured impedance data into a data format suitable for automated further processing. The output structure is a table containing an electrochemical impedance spectroscopy measurement in each row. Detailed technical explanations can be found in the corresponding open-source repository [19]. Most processing steps are parallelized by splitting up the data among all available kernels of the host machine to increase the processing speed. The data processing can be split into four significant steps, as shown schematically in Fig. 4.

In the initial data preparation step, the electrochemical impedance spectroscopy measurements are filtered and aligned concerning the measured frequencies. Further features are extracted from the measurements and added as information after interpolating all measurements to the same set of frequencies. Furthermore, additional features are extracted and added as information to the measurement table during the pre-evaluation process. The data is plotted as a next step to enable humans to interpret the data. As an example of the usage of this tool, a regression model is developed to determine the temperature based on impedance measurements of a battery.

3.1. Data preparation and pre-evaluation

As the excitation frequencies of electrochemical impedance spectroscopy measurements from different laboratories and devices differ, they are harmonized in the first step. Therefore a new frequency range from $f_{\mathrm{min,\ new}}$ to $f_{\mathrm{max,\ new}}$ is selected. All the measurements that should be further processed must cover at least that bandwidth to avoid extrapolation. The tool offers three methods. First, hard coding all frequencies that should be used. Second, manual selection of $f_{\mathrm{min,\ new}}$, $f_{\mathrm{max,\ new}}$ and how many frequencies per decade logarithmic distributed the new frequency set should have. The third option scans the provided data for all frequency groups and lists them by percentage use, which can then be selected.

Even if the effectiveness is mathematically disproved [35], the linear Kramers-Kronig validity test [23,36] is applied to all measurements. The maximum absolute error of the linear Kramers-Kronig results is calculated as a single scalar error metric for every measurement. An interactive plot is provided to set the maximum acceptable error threshold. For the interpolation of all electrochemical impedance spectroscopy measurements, the SciPy [37] implementation of the piecewise cubic hermite interpolating polynomial one-dimensional monotonic cubic interpolation [38] is used. Afterward, a 2D table format is generated, containing one complete electrochemical impedance spectroscopy measurement and its additional labels and features in each row. Each frequency is transformed into four columns to store cartesian and polar values directly.

In many publications, equivalent circuit models are fitted to electrochemical impedance spectroscopy curves to extract features. If only one cell type is used, the components used for the equivalent circuit model can be adapted to the changes in the battery. Generally, the choice of elements can lead to precise but ambiguous parameters [39]. The components for all batteries strongly depend on the measured frequency range. If, for example, frequencies in the megahertz range are measured as well, different elements have to be chosen [40]. This tool uses the existing library from Murbach et al. (2020) [23] to fit one freely chooseable circuit to all measurements. The fitted parameters are added as columns to the data table.

The distribution of relaxation times analysis of electrochemical impedance spectroscopy data is equivalent to equivalent circuit model fitting with distributions of resistor-capacitor elements [41]. This tool uses the implementation by Liu and Ciucci (2020) [24] to calculate the distribution of relaxation times. The complete distribution of relaxation times is not saved and added here to the table. Instead, up to ten peaks of the distribution of relaxation times are calculated, and their time constant and amplitude are stored in the data table.

The last preparation and pre-evaluation step is calculating extrema and zero crossings in the Bode and Nyquist diagrams. The bode diagrams, absolute values, and the phase are searched separately for minima and maxima. Up to three coordinates are saved for every search for extrema and zero crossings.

3.2. Data inspection and visualization

Besides plotting typical figures like Nyquist and Bode (see, e.g., Fig. 2) diagrams, further first correlation dependencies can be visually extracted. The statistics help the users to recognize dependencies and thus select variables on which to construct models. The coverage of the value range, e.g., the temperature of the measurements, can also be analyzed in more detail. In the following, an exemplary exploratory data analysis on the example data is conducted to uncover patterns, anomalies, and insights from the data. This process involves statistical summaries, correlation analysis, and the generation of visualizations to understand the data's characteristics better. The example data covers a wide range of temperatures and state-of-charges, but no aging.

An example of a possible diagram is given in Fig. 5. The figure is a grid with five rows and five columns. Each row and column corresponds to a different variable. The exemplary selected variables are state-of-charge in percent, R_0 of an equivalent circuit model fit in Ohm, Time Constant τ of the first peak of the distribution of relaxation times in seconds, Temperature in °C, and the Frequency of the first minimum of the phase in Hertz. The diagonal plots represent each variable's distribution, generally shown as histograms and with Gaussian kernel density estimations. The distributions can provide insights into each variable's range, central tendency, and spread of values. They can also reveal any skewness or presence of outliers.

The contour plots in the lower triangle of Fig. 5 represent the joint distribution of two variables. The areas where the contour lines are red indicate where data points are most concentrated. For instance, the contour plot between R_0 and state-of-charge shows a multi-modal

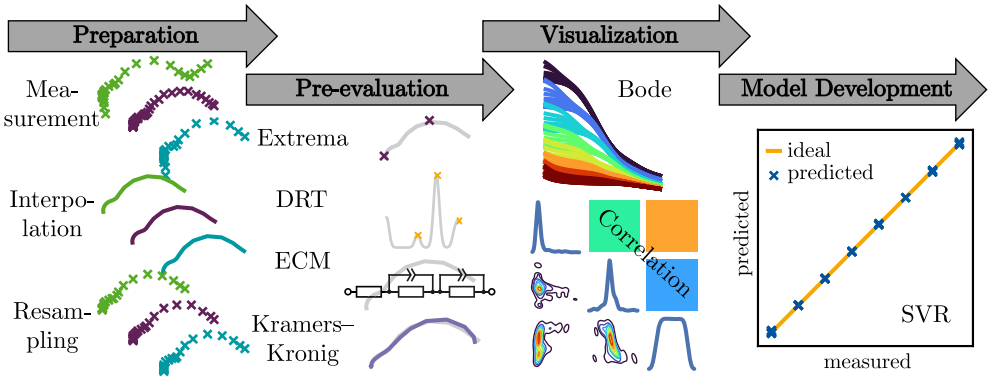

Fig. 4. Processing steps of the *EIS Data Analytics* tool. After aligning the frequencies measured by interpolation and resampling, further features by pre-evaluation are added to the individual electrochemical impedance spectroscopy (EIS) measurements. The additional features include an analysis of the distribution of relaxation timess (DRTs) and equivalent circuit models (ECMs). The gathered data can be visualized in different ways. Finally, a model can be derived from the data. This publication presents an support vector regression (SVR) model for temperature estimation.

distribution, suggesting different clusters or groupings in the data. The contour plot of the multi-modal distribution of the state-of-charge and the temperature shows the test matrix of the recorded impedance measurements. The colored squares on the upper triangle represent the Pearson correlation coefficient (r) between pairs of variables. This coefficient ranges from −1 to 1, where 1 means perfect positive correlation, −1 means perfect negative correlation, and 0 means no linear correlation. For example, the correlation between temperature and the frequency of the first minimum of the phase is $r = 0.73$, indicating a positive linear relationship.

3.3. Model development

After restructuring the data and performing a detailed visual inspection, a model fitting the data can be applied. This paper exemplary uses support vector machine regression with an radial basis function kernel to estimate the cell temperature at various state-of-charges with interpolation capabilities. The possibility of extrapolation is not investigated. In the shared repository [19], the reader can apply different kernels or fit for other features. Hyperparameter optimization is implemented as the choice of hyperparameters is crucial for the regression result [42]. The hyperparameters are optimized within the following ranges: $\gamma \in [0.001, 100]$, tolerance $\in [0.001, 10]$, $C \in [0.01, 10000000000]$ and $\varepsilon \in [0.01, 10]$. For each of the following models, in this parameter space of γ, tolerance, C and ε, at least 30.000 parameter combinations are tested. The parameters are selected randomly by a reciprocal distribution, also known as the log-uniform distribution. The parameter range is selected so that the optimal choice converges to a global optimal choice, as later explained.

The data is first scaled before fitting. The reactivity of a battery, and thus also its impedance, generally shows an Arrhenius-like dependence [43,44]. Therefore, the absolute values of the impedance data are first scaled:

$$|\underline{Z}|_{\text{scaled,Arrhenius}} = \log\left(\frac{1}{|\underline{Z}|}\right). \tag{1}$$

Afterwards the value range is additionally limited to $[0, 1]$ with a so-called min–max scaling:

$$|\underline{Z}|_{\text{scaled}} = \frac{|\underline{Z}|_{\text{scaled,Arrhenius}} - \min\left(|\underline{Z}|_{\text{scaled,Arrhenius}}\right)}{\max\left(|\underline{Z}|_{\text{scaled,Arrhenius}}\right) - \min\left(|\underline{Z}|_{\text{scaled,Arrhenius}}\right)}. \tag{2}$$

For all regression results, only the absolute value of the impedance is used as an input. Also, for all regressions, the dataset is split up as follows. The electrochemical impedance spectroscopy measurements at 5 °C and 35 °C are excluded from the dataset and are being used for testing. However, this enables interpolation to be checked but not extrapolation. The remaining measurements are split up randomly into 80% data for training and 20% for validation. As a first step, only individual frequencies of the complete spectra are fitted. By this, overfitting and underfitting can still be visualized [45]. Afterwards, the full spectra are used.

As a first step the absolute values of impedance of the frequencies $f = 0.01\,\text{Hz}, 1.1086\,\text{Hz} \approx 1\,\text{Hz}$ and $93.1702\,\text{Hz} \approx 100\,\text{Hz}$ are used as model input. The temperature during the electrochemical impedance spectroscopy measurement is used for the model output. Fig. 6 shows the result of the fitted support vector regression models. In the upper row of the figure, a sweep of the impedance values is used as an input of the final model to create the purple-colored support vector regression line. The second row indicates the difference between the actual temperature during the measurement on the x-axis and the predicted measurement on the y-axis. All estimations would be on the green ideal line for a perfect model.

The found optimum for the 0.01 Hz fit on the left side uses the following parameters: $\gamma \approx 3.30 \cdot 10^{-1}$, tolerance $\approx 3.00 \cdot 10^{-3}$, $C \approx 1.43 \cdot 10^{7}$ and $\varepsilon \approx 4.20 \cdot 10°$. The best overall mean-square-error calculated as the maxima of the mean-square-errors of the train, validation, and test dataset is $23.14\,\text{K}^2$. The optimization of the hyperparameter is further explained later for complete spectra. The optimum for the 1 Hz fit in the middle of Fig. 6, is found for the following parameters: $\gamma \approx 1.53 \cdot 10°$, tolerance $\approx 2.56 \cdot 10°$, $C \approx 4.81 \cdot 10^{4}$ and $\varepsilon \approx 1.28 \cdot 10°$. The best overall mean-square-error is $7.27\,\text{K}^2$. For the 100 Hz fit on the right side of Fig. 6, the following parameters are used: $\gamma \approx 4.96 \cdot 10°$, tolerance $\approx 2.69 \cdot 10^{-3}$, $C \approx 2.80 \cdot 10^{6}$ and $\varepsilon \approx 7.18 \cdot 10^{-1}$. The best overall mean-square-error is $0.75\,\text{K}^2$.

As Figs. 2 and 3 show, the time constants of the battery processes are changing, especially in the middle-frequency range. Thus, the sensitivity of individual frequencies changes with the temperature range. This results in good results for individual frequencies, as shown above, but it does not exploit the full potential for all the temperature ranges measured. As a next step, the entire spectrum of the absolute value of the measured impedance is used as input. The hyperparameter selection and the division of the data into test and train data sets are carried out in the same way as for the individual frequencies.

The result of the hyperparameter search for the model using the complete spectra is given in Fig. 7. For the used metrics, the mean-square-error, the optimal result is found for $\gamma \approx 6.60 \cdot 10^{-2}$, tolerance $\approx 9.88 \cdot 10^{-1}$, $C \approx 3.85 \cdot 10^{5}$ and $\varepsilon \approx 1.66 \cdot 10^{-1}$ with an overall mean-square-error of $0.10\,\text{K}^2$. As mentioned, at least 30.000 parameter combinations were evaluated for each presented model. The parameters are selected randomly with a logarithmic uniform distribution. In Fig. 7, concave hulls are used to draw the parameter space. The x-axes are limited to a mean-square-error of $200\,\text{K}^2$. For the parameter combinations tested here, Fig. 7 indicates that the selected combination is an optimum.

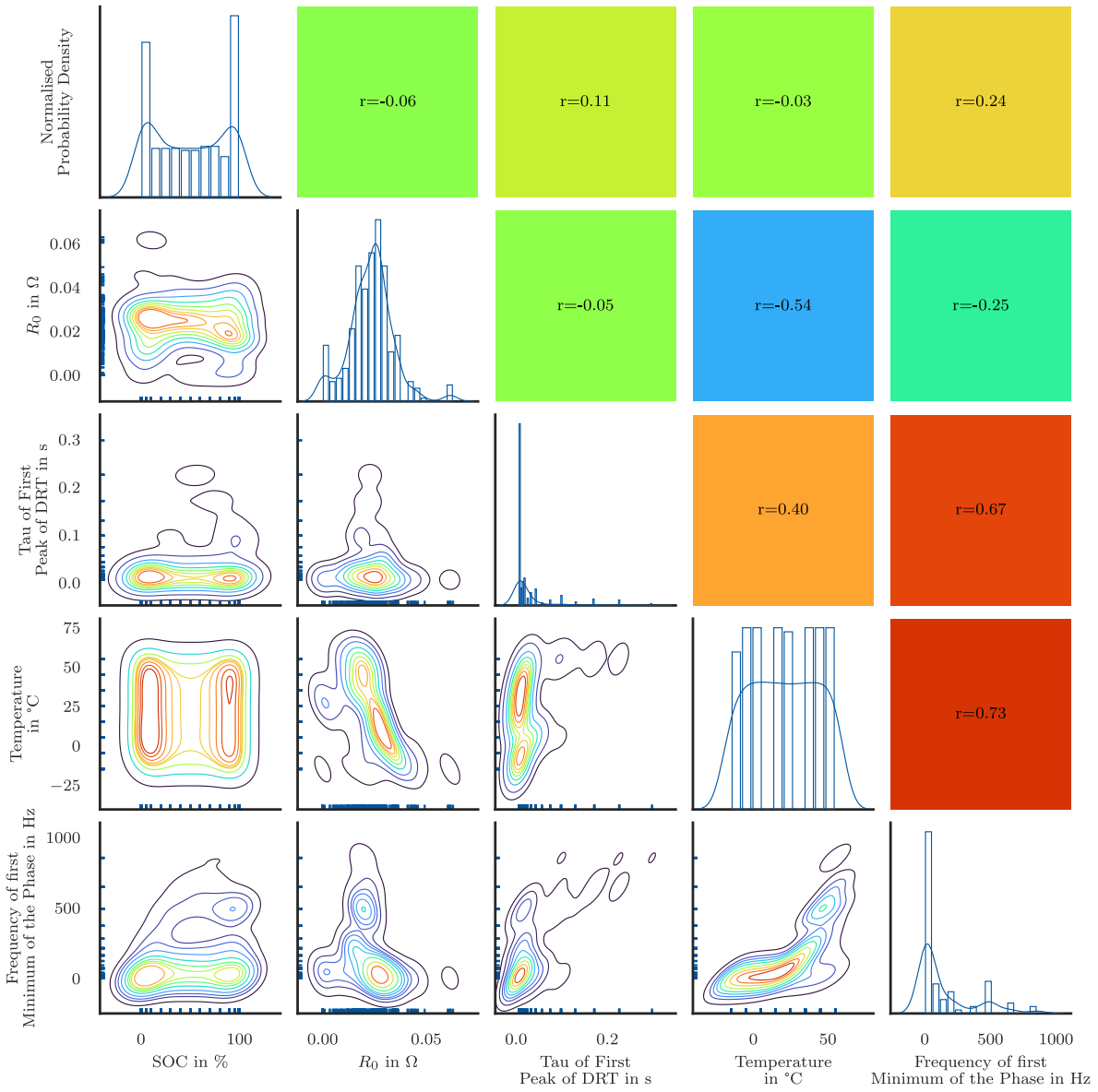

Fig. 5. Correlation analysis of the state-of-charge (SOC) of the battery, R_0 of an equivalent circuit model (ECM) fit, $\tau_{\text{FirstPeak}}$ of the distribution of relaxation times (DRT), the temperature of the battery and the frequency of the first minimum of the impedance phase. The diagonal shows histograms with Gaussian kernel density estimations. The lower triangle displays contour lines of the joint distributions. In the upper triangle, the scalar Person correlation coefficient is given. (For interpretation of the references to color in this figure legend, the reader is referred to the web version of this article.)

Other parameters would lead to worse results, especially for the test results.

Different from Fig. 6 for the individual frequencies, only the scatter plot can now be given, which shows the difference in the model output. Fig. 8 shows the predicted temperature on the y-axis and, on the x-axis, the actual temperature of the battery during the impedance measurement. The temperature of the electrochemical impedance spectroscopy measurements was measured and actively controlled by ten DS18B20U+ sensors from Analog Devices, beforehand Maxim Integrated. A single sensor guarantees an absolute error of less than 0.5 K for the measurements, apart from the one at −15 °C.

4. Discussion

The example data set only covers a temperature change and state-of-charge. This is sufficient to develop and explain the tool. Nevertheless, in Section 4.1, verification is done by reproducing another publication. This work provides a basis for further, more complex analyses and developments. The automatic harmonization of different measurements into one format is essential and new for an open-source tool. Cell and cross-laboratory analyses are thus possible.

The support vector regression with an radial basis function kernel for temperature estimation results in promising mean-square-errors. The impact of different aging paths on the results is not covered in this publication, but it is necessary to ensure that the accuracy is maintained in the application. If the accuracy remains similar for further variations of external or internal changes to the battery, the question of integrability into the application arises.

The temperature of the reference data was measured with ten sensors. A single sensor guarantees an absolute error of less than 0.5 K for the measurements, apart from the one at −15 °C according to the data sheet. The achieved mean-square-error of 0.10 K^2 for the temperature estimation, based on the complete spectra, is thus in a reasonable range.

Fig. 7 suggests that the chosen hyperparameters are a global optimum. Nevertheless, the same method was also applied to the individual frequency of 100 Hz as shown in Fig. 6 on the right side. Notably, the

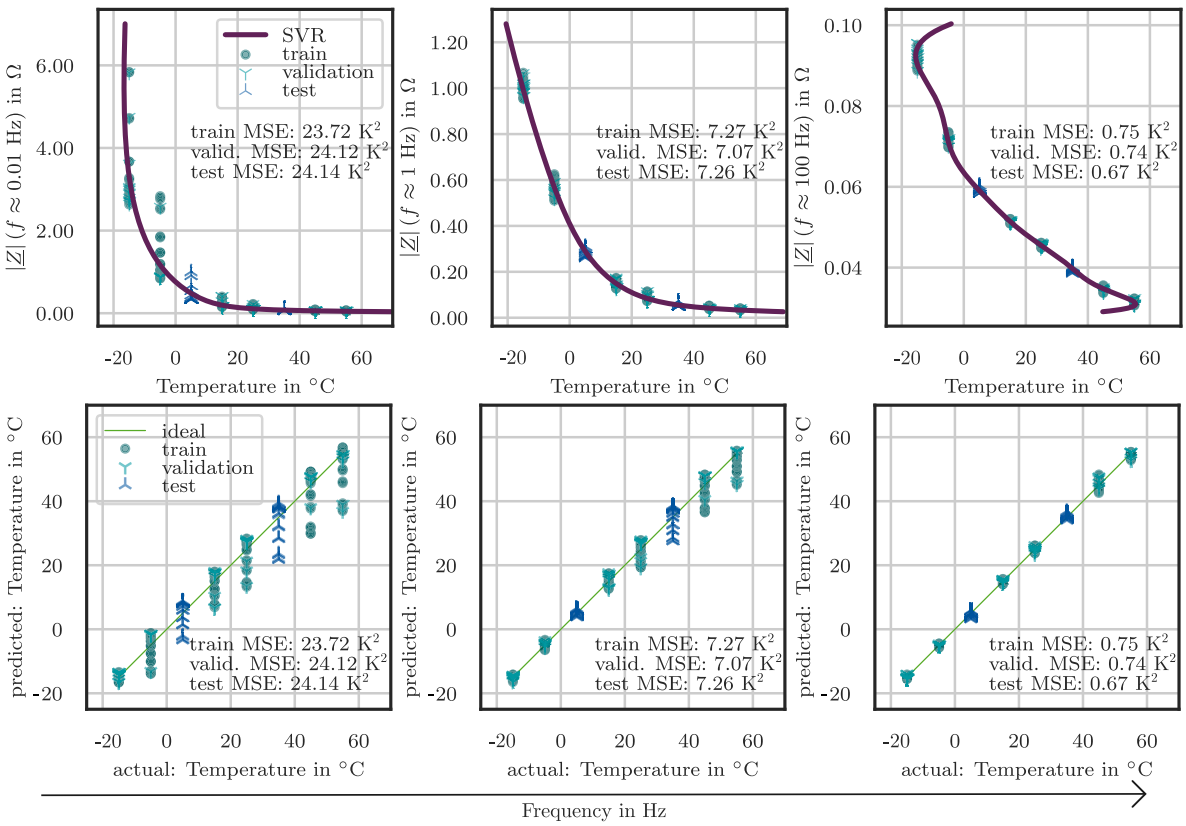

Fig. 6. Fitting result of a support vector regression (SVR) for temperature prediction based on the absolute value of the impedance of individual frequencies. Three frequencies are evaluated: 0.01 Hz, 1.1086 Hz ≈ 1 Hz and 93.1702 Hz ≈ 100 Hz. The lowest mean-square-error (MSE) is given for 100 Hz. The first row shows the evaluation of the per frequency fitted support vector regression model with the temperature during the electrochemical impedance spectroscopy (EIS) measurement on the x-axis. The second row shows the predicted temperature on the y-axis, and the x-axes show the actual temperature of the battery during the impedance measurement.

selection of the parameters chosen here is only optimal for the given data and the selected constraints, namely interpolability. The 100 Hz results show that already slight extrapolation can lead to high errors. Future improvements could be achieved by testing the models with physical–chemical model-based extrapolation results. This would allow combining the low mean-square-error achieved by support vector regression for interpolation and the extrapolability of physical–chemical models.

Reducing the complexity of the models would result in lower requirements for integration. A statistical, mathematical analysis, e.g., applying the analysis of variance (ANOVA) or principal component analysis (PCA), could provide further information about the necessary frequency range. This could reduce the dimension of the input data. On the other hand, the complexity could also be increased to allow for cell-independent models. If a generally applicable model could be found, the integration into an application-specific integrated circuit (ASIC) of the battery management system (BMS) is enabled.

4.1. Verification

In the publication of Faraji-Niri et al. (2023) [31] the state-of-health is predicted based on impedance data. The prediction uses machine learning, namely a Gaussian process regression model together with a Bayesian optimization method. The data is published in Rashid et al. (2023) [32] and consists of 360 electrochemical impedance spectroscopy measurements of cylindrical 21 700 NMC 811 cells. The measurements cover the following range of parameters: Temperatures: 15, 25 and 35 °C, state-of-charges: 5, 20, 50, 70 and 95% and state-of-healths: 80, 85, 90, 95 and 100%. In case study 1 of the publication [31] beside the electrochemical impedance spectroscopy measurements also, the temperature and the state-of-charges are used as input for the model. The mean-square-error of the estimation of the state-of-health is 1.0374%² [31].

With the here presented *EIS Data Analytics* [19] tool the case study 1 of Faraji-Niri et al. (2023) [31] is recreated. Furthermore, the number of inputs is reduced to case B with only the absolute values of the impedance as input, and case C with the absolute values as well as the temperature and the state-of-charge. The previously described approach for the temperature estimation is slightly adapted to the extended input data. The absolute values are still scaled with the Arrhenius correction of Eq. (1). The other input values are only modified by a min–max scaling. As the dataset is more diverse but less dense, similar to the approach of Faraji-Niri et al. the data is randomly split in 20% for validation and 80% for training. The hyperparameters are optimized in the same range as before and again with 30.000 randomly selected combinations. For case B the mean-square-error for the best parameter combination is 2.49%². In case C the mean-square-error for the best parameter combination is 1.51%². For the selection of input values, identical to case study 1 of Faraji-Niri et al. an mean-square-error of 2.19%² is achieved. The small difference in the error verifies, on the one hand, the results of Faraji-Niri et al. (2023) [31], and on the other hand shows the flexibility and performance of the here presented tool. With specific optimizations, such as optimization for interpolation, this might be further reduced. More details, including figures like Figs. 7 and 8 of the verification can be found in the related repository: https://git.rwth-aachen.de/isea/eis_data_analytics.

5. Conclusions

This tool enables more efficient and detailed analysis of electrochemical impedance data. It provides insights into the possibilities of impedance evaluation using temperature estimation as an example.

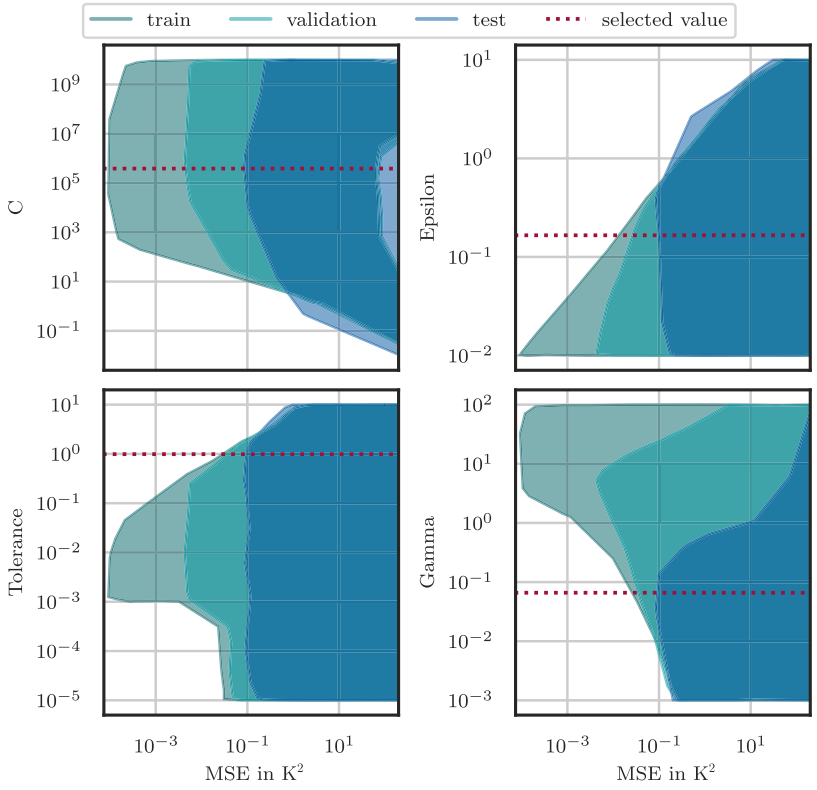

Fig. 7. Hyperparameter optimization results of 30.000 different parameter combinations for a support vector regression (SVR) approach of electrochemical impedance spectroscopy (EIS) based temperature estimation. The smallest mean-square-error (MSE) is given for $\gamma \approx 6.60 \cdot 10^{-2}$, tolerance $\approx 9.88 \cdot 10^{-1}$, $C \approx 3.85 \cdot 10^{5}$ and $\epsilon \approx 1.66 \cdot 10^{-1}$. The best overall mean-square-error calculated as the maxima of the mean-square-errors of the train, validation and test dataset, is $0.10\,\mathrm{K}^2$.

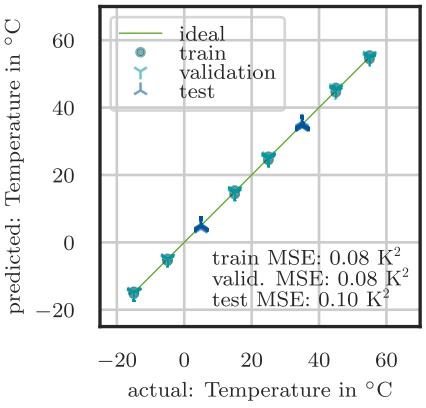

Fig. 8. Results of a support vector regression (SVR) with radial basis function (RBF) kernel using the absolute values of an electrochemical impedance spectroscopy (EIS) spectra as input data and predicting the temperature. The *y*-axis shows the predicted temperature, and the *x*-axis shows the actual temperature of the battery during the impedance measurement.

The ability to first harmonize data and then automate the analysis process for electrochemical impedance spectroscopy measurements meets a critical need in electrochemical energy storage and conversion systems. By integrating various analysis methods, such as equivalent circuit model, distribution of relaxation times, linear Kramers-Kronig, and support vector regression for impedance-based estimation, the tool improves the precision of impedance-based evaluation under various conditions. In addition, it is entirely open-source to encourage collaborative improvements and customization, which can accelerate innovation in electrochemical research.

The dataset provided only covers temperature and state-of-charge changes and serves as a basis for the development of the tool. Future work should aim to expand the scope of the analysis to account for different aging pathways, different cells, and other external or internal changes to the battery. This extension is necessary to verify the applicability and accuracy of the tool and the methods used under a broader range of conditions.

The promising results obtained in temperature estimation using support vector regression indicate that the tool can potentially improve the precision and reliability of battery diagnostics and prognostics. More precise temperature measurements in applications can reduce costs by minimizing the safety margins to critical limits. Moreover, critical values can be detected earlier if the temperature of all cells is known by measuring the impedance. However, further validations and refinements are required to realize its full potential, mainly to ensure its applicability to various battery types and conditions. Integrating the models into application-specific integrated circuits for battery management systems should also be investigated, which could significantly improve the functionality and safety of electrochemical energy storage systems.

CRediT authorship contribution statement

Alexander Blömeke: Writing – original draft, Visualization, Validation, Supervision, Software, Resources, Project administration, Methodology, Investigation, Formal analysis, Data curation, Conceptualization. **Ole Kappelhoff:** Writing – review & editing, Validation, Software, Resources, Methodology, Investigation, Formal analysis, Data curation, Conceptualization. **David Wasylowski:** Writing – review & editing, Supervision, Resources, Project administration, Funding acquisition. **Florian Ringbeck:** Writing – review & editing, Supervision, Resources, Project administration, Funding acquisition. **Dirk Uwe Sauer:** Writing – review & editing, Supervision, Resources, Project administration, Funding acquisition.

Declaration of competing interest

The authors declare the following financial interests/personal relationships which may be considered as potential competing interests: The authors declare that they have no competing interests beside the funding mentioned in the acknowledgments.

Data availability

Data is available:

EIS Data Analytics (Original data) (RWTH Publications)
EIS Data Analytics (Original data) (RWTH Aachen University GitLab)

Declaration of Generative AI and AI-assisted technologies in the writing process

During the preparation of this work, the authors used ChatGPT-4, Grammarly Premium, DeepL, and Copilot Pro to improve the readability. After using these tools/services, the authors reviewed and edited the content as needed and take full responsibility for the content of the publication.

Acknowledgments

The project DEAL enabled and organized open-access funding. This research received funding from the Federal Ministry of Education and Research (BMBF), Germany in the project OSLiB (funding code: 03XP0330C).

References

[1] O. Kanoun, J. Himmel, A. Errachid, Impedance spectroscopy and its application in measurement and sensor technology, Appl. Sci. 13 (1) (2023) 244, http://dx.doi.org/10.3390/app13010244, URL: https://www.mdpi.com/2076-3417/13/1/244.

[2] A.H. Ismail, T. Gross, G. Schlieper, M. Walter, F. Eitner, J. Floege, S. Leonhardt, Monitoring transcellular fluid shifts during episodes of intradialytic hypotension using bioimpedance spectroscopy, Clin. Kidney J. 14 (1) (2021) 149–155, http://dx.doi.org/10.1093/ckj/sfz123, URL: https://academic.oup.com/ckj/article/14/1/149/5571149.

[3] W. Hu, Y. Peng, Y. Wei, Y. Yang, Application of electrochemical impedance spectroscopy to degradation and aging research of Lithium-ion batteries, J. Phys. Chem. C 127 (9) (2023) 4465–4495, http://dx.doi.org/10.1021/acs.jpcc.3c00033, URL: https://pubs.acs.org/doi/10.1021/acs.jpcc.3c00033.

[4] O. Bohlen, Impedance Based Battery Monitoring (Ph.D. thesis), Shaker, Aachen, 2008, http://dx.doi.org/10.18154/RWTH-CONV-113079, URL: http://publications.rwth-aachen.de/record/50539.

[5] J.P. Schmidt, S. Arnold, A. Loges, D. Werner, T. Wetzel, E. Ivers-Tiffée, Measurement of the internal cell temperature via impedance: Evaluation and application of a new method, J. Power Sources 243 (2013) 110–117, http://dx.doi.org/10.1016/j.jpowsour.2013.06.013, URL: https://www.sciencedirect.com/science/article/pii/S0378775313010070.

[6] M. Kwiecien, Electrochemical Impedance Spectroscopy on Lead-Acid Cells During Aging (Ph.D. thesis), ISEA, 2019, http://dx.doi.org/10.18154/RWTH-2019-09480, URL: https://publications.rwth-aachen.de/record/768701.

[7] T. Rüther, C. Plank, M. Schamel, M.A. Danzer, Detection of inhomogeneities in serially connected lithium-ion batteries, Appl. Energy 332 (2023) 120514, http://dx.doi.org/10.1016/j.apenergy.2022.120514, URL: https://www.sciencedirect.com/science/article/pii/S0306261922017718.

[8] H. Zappen, F. Ringbeck, D.U. Sauer, Application of time-resolved multi-sine impedance spectroscopy for Lithium-ion battery characterization, Batteries 4 (4) (2018) 64, http://dx.doi.org/10.3390/batteries4040064, URL: https://www.mdpi.com/2313-0105/4/4/64.

[9] A. Straßer, A. Adam, J. Li, In operando detection of Lithium plating via electrochemical impedance spectroscopy for automotive batteries, J. Power Sources 580 (2023) 233366, http://dx.doi.org/10.1016/j.jpowsour.2023.233366, URL: https://www.sciencedirect.com/science/article/pii/S0378775323007425.

[10] A.S. Mussa, M. Klett, G. Lindbergh, R.W. Lindström, Effects of external pressure on the performance and ageing of single-layer lithium-ion pouch cells, J. Power Sources 385 (2018) 18–26, http://dx.doi.org/10.1016/j.jpowsour.2018.03.020, URL: https://www.sciencedirect.com/science/article/pii/S0378775318302441.

[11] V. Müller, R.-G. Scurtu, M. Memm, M.A. Danzer, M. Wohlfahrt-Mehrens, Study of the influence of mechanical pressure on the performance and aging of Lithium-ion battery cells, J. Power Sources 440 (2019) 227148, http://dx.doi.org/10.1016/j.jpowsour.2019.227148, URL: https://www.sciencedirect.com/science/article/pii/S0378775319311413.

[12] F.J. Günter, J.B. Habedank, D. Schreiner, T. Neuwirth, R. Gilles, G. Reinhart, Introduction to electrochemical impedance spectroscopy as a measurement method for the wetting degree of Lithium-ion cells, J. Electrochem. Soc. 165 (14) (2018) A3249–A3256, http://dx.doi.org/10.1149/2.0081814jes, URL: https://iopscience.iop.org/article/10.1149/2.0081814jes.

[13] S. Käbitz, Untersuchung der Alterung von Lithium-Ionen-Batterien mittels Elektroanalytik und elektrochemischer Impedanzspektroskopie (Ph.D. thesis), RWTH Aachen University, 2016, http://dx.doi.org/10.18154/RWTH-2016-12094, URL: http://publications.rwth-aachen.de/record/680923.

[14] S.E.J. O'Kane, W. Ai, G. Madabattula, D. Alonso-Alvarez, R. Timms, V. Sulzer, J.S. Edge, B. Wu, G.J. Offer, M. Marinescu, Lithium-ion battery degradation: how to model it, Phys. Chem. Chem. Phys. 24 (13) (2022) 7909–7922, http://dx.doi.org/10.1039/D2CP00417H, URL: https://pubs.rsc.org/en/content/articlelanding/2022/cp/d2cp00417h.

[15] F. Frie, H. Ditler, S. Klick, G. Stahl, C. Rahe, T. Ghaddar, D.U. Sauer, An analysis of calendaric aging over 5 years of Ni-rich 18650-cells with Si/C anodes, ChemElectroChem 11 (9) (2024) e202400020, http://dx.doi.org/10.1002/celc.202400020, URL: https://onlinelibrary.wiley.com/doi/abs/10.1002/celc.202400020.

[16] N. Meddings, M. Heinrich, F. Overney, J.-S. Lee, V. Ruiz, E. Napolitano, S. Seitz, G. Hinds, R. Raccichini, M. Gaberš˘ cek, J. Park, Application of electrochemical impedance spectroscopy to commercial Li-ion cells: A review, J. Power Sources 480 (2020) 228742, http://dx.doi.org/10.1016/j.jpowsour.2020.228742, URL: https://www.sciencedirect.com/science/article/pii/S0378775320310466.

[17] K.M. Carthy, H. Gullapalli, K.M. Ryan, T. Kennedy, Review—Use of impedance spectroscopy for the estimation of Li-ion battery state of charge, state of health and internal temperature, J. Electrochem. Soc. 168 (8) (2021) 080517, http://dx.doi.org/10.1149/1945-7111/ac1a85.

[18] N. Hallemans, D. Howey, A. Battistel, N.F. Saniee, F. Scarpioni, B. Wouters, F. La Mantia, A. Hubin, W.D. Widanage, J. Lataire, Electrochemical impedance spectroscopy beyond linearity and stationarity—A critical review, Electrochim. Acta 466 (2023) 142939, http://dx.doi.org/10.1016/j.electacta.2023.142939, URL: https://www.sciencedirect.com/science/article/pii/S0013468623011143.

[19] A. Blömeke, O. Kappelhoff, D.U. Sauer, EIS data analytics; v0.0.9, 2024, http://dx.doi.org/10.18154/RWTH-2024-03849, URL: https://git.rwth-aachen.de/isea/eis_data_analytics.

[20] Y. Zhang, Q. Tang, Y. Zhang, J. Wang, U. Stimming, A.A. Lee, Identifying degradation patterns of lithium ion batteries from impedance spectroscopy using machine learning, Nature Commun. 11 (1) (2020) 1706, http://dx.doi.org/10.1038/s41467-020-15235-7, URL: https://www.nature.com/articles/s41467-020-15235-7.

[21] P. Gasper, A. Schiek, K. Smith, Y. Shimonishi, S. Yoshida, Predicting battery capacity from impedance at varying temperature and state of charge using machine learning, Cell Rep Phys Sci 3 (12) (2022) 101184, http://dx.doi.org/10.1016/j.xcrp.2022.101184, URL: https://www.sciencedirect.com/science/article/pii/S2666386422005021.

[22] K. Knudsen, Kbknudsen/PyEIS: PyEIS: A python-based electrochemical impedance spectroscopy simulator and analyzer, 2019, http://dx.doi.org/10.5281/zenodo.2535951, URL: https://zenodo.org/records/2535951.

[23] M.D. Murbach, B. Gerwe, N. Dawson-Elli, L.-k. Tsui, impedance.py: A Python package for electrochemical impedance analysis, J. Open Source Softw. 5 (52) (2020) 2349, http://dx.doi.org/10.21105/joss.02349, URL: https://joss.theoj.org/papers/10.21105/joss.02349.

[24] J. Liu, F. Ciucci, The Gaussian process distribution of relaxation times: A machine learning tool for the analysis and prediction of electrochemical impedance spectroscopy data, Electrochim. Acta 331 (2020) 135316, http://dx.doi.org/10.1016/j.electacta.2019.135316, URL: https://www.sciencedirect.com/science/article/pii/S0013468619321887.

[25] V. Yrjänä, DearEIS - a GUI program for analyzing impedance spectra, J. Open Source Softw. 7 (80) (2022) 4808, http://dx.doi.org/10.21105/joss.04808, URL: https://joss.theoj.org/papers/10.21105/joss.04808.

[26] R.R. Richardson, P.T. Ireland, D.A. Howey, Battery internal temperature estimation by combined impedance and surface temperature measurement, J. Power Sources 265 (2014) 254–261, http://dx.doi.org/10.1016/j.jpowsour.2014.04.129, URL: https://www.sciencedirect.com/science/article/pii/S0378775314006302.

[27] H.P.G.J. Beelen, L.H.J. Raijmakers, M.C.F. Donkers, P.H.L. Notten, H.J. Bergveld, A comparison and accuracy analysis of impedance-based temperature estimation methods for Li-ion batteries, Appl. Energy 175 (2016) 128–140, http://dx.doi.org/10.1016/j.apenergy.2016.04.103, URL: https://www.sciencedirect.com/science/article/pii/S0306261916305621.

[28] X. Wang, X. Wei, Q. Chen, J. Zhu, H. Dai, Lithium-ion battery temperature on-line estimation based on fast impedance calculation, J. Energy Storage 26 (2019) 100952, http://dx.doi.org/10.1016/j.est.2019.100952, URL: https://www.sciencedirect.com/science/article/pii/S2352152X19306681.

[29] L. Wang, D. Lu, M. Song, X. Zhao, G. Li, Instantaneous estimation of internal temperature in lithium-ion battery by impedance measurement, Int. J. Energy Res. 44 (4) (2020) 3082–3097, http://dx.doi.org/10.1002/er.5144, URL: https://onlinelibrary.wiley.com/doi/abs/10.1002/er.5144.

[30] K. Mc Carthy, H. Gullapalli, T. Kennedy, Real-time internal temperature estimation of commercial Li-ion batteries using online impedance measurements, J. Power Sources 519 (2022) 230786, http://dx.doi.org/10.1016/j.jpowsour.2021.230786, URL: https://www.sciencedirect.com/science/article/pii/S0378775321012775.

[31] M. Faraji-Niri, M. Rashid, J. Sansom, M. Sheikh, D. Widanage, J. Marco, Accelerated state of health estimation of second life lithium-ion batteries via electrochemical impedance spectroscopy tests and machine learning techniques, J. Energy Storage 58 (2023) 106295, http://dx.doi.org/10.1016/j.est.2022.106295, URL: https://www.sciencedirect.com/science/article/pii/S2352152X22022848.

[32] M. Rashid, M. Faraji-Niri, J. Sansom, M. Sheikh, D. Widanage, J. Marco, Dataset for rapid state of health estimation of lithium batteries using EIS and machine learning: Training and validation, Data Brief 48 (2023) 109157, http://dx.doi.org/10.1016/j.dib.2023.109157, URL: https://www.sciencedirect.com/science/article/pii/S2352340923002767.

[33] S.E. Ezahedi, M. Kharrich, J. Kim, Multi-cell sensorless internal temperature estimation based on electrochemical impedance spectroscopy with Gaussian process regression for lithium-ion batteries safety, J. Energy Storage 94 (2024) 112467, http://dx.doi.org/10.1016/j.est.2024.112467, URL: https://www.sciencedirect.com/science/article/pii/S2352152X2402053X.

[34] Y. Liu, L. Yang, R. Liao, C. Hu, Y. Xiao, J. Wu, C. He, Y. Zhang, S. Li, Data-driven internal temperature estimation methods for sodium-ion battery using electrochemical impedance spectroscopy, J. Energy Storage 87 (2024) 111426, http://dx.doi.org/10.1016/j.est.2024.111426, URL: https://www.sciencedirect.com/science/article/pii/S2352152X24010119.

[35] T. Heil, Ersatzschaltbild-basierte Modellierung der Diffusion und des Ladungsdurchtritts in Lithium-Ionen-Zellen (Ph.D. thesis), Technische Universität München, 2020, URL: https://nbn-resolving.de/urn/resolver.pl?urn:nbn:de:bvb:91-diss-20201217-1575045-1-4.

[36] M. Schönleber, D. Klotz, E. Ivers-Tiffée, A method for improving the robustness of linear Kramers–Kronig validity tests, Electrochim. Acta 131 (2014) 20–27, http://dx.doi.org/10.1016/j.electacta.2014.01.034, URL: https://www.sciencedirect.com/science/article/pii/S0013468614001005.

[37] P. Virtanen, R. Gommers, T.E. Oliphant, M. Haberland, T. Reddy, D. Cournapeau, E. Burovski, P. Peterson, W. Weckesser, J. Bright, S.J. van der Walt, M. Brett, J. Wilson, K.J. Millman, N. Mayorov, A.R.J. Nelson, E. Jones, R. Kern, E. Larson, C.J. Carey, I. Polat, Y. Feng, E.W. Moore, J. VanderPlas, D. Laxalde, J. Perktold, R. Cimrman, I. Henriksen, E.A. Quintero, C.R. Harris, A.M. Archibald, A.H. Ribeiro, F. Pedregosa, P. van Mulbregt, SciPy 1.0 Contributors, SciPy 1.0: Fundamental algorithms for scientific computing in python, Nat. Methods 17 (2020) 261–272, http://dx.doi.org/10.1038/s41592-019-0686-2, URL: https://www.nature.com/articles/s41592-019-0686-2.

[38] F.N. Fritsch, J. Butland, A method for constructing local monotone piecewise cubic interpolants, SIAM J. Sci. Stat. Comput. 5 (2) (1984) 300–304, http://dx.doi.org/10.1137/0905021, URL: https://epubs.siam.org/doi/10.1137/0905021. Publisher: Society for Industrial and Applied Mathematics.

[39] M. Gaberšček, Understanding Li-based battery materials via electrochemical impedance spectroscopy, Nature Commun. 12 (1) (2021) 6513, http://dx.doi.org/10.1038/s41467-021-26894-5, URL: https://www.nature.com/articles/s41467-021-26894-5. Number: 1 Publisher: Nature Publishing Group.

[40] T.F. Landinger, G. Schwarzberger, A. Jossen, High frequency impedance characteristics of cylindrical lithium-ion cells: Physical-based modeling of cell state and cell design dependencies, J. Power Sources 488 (2021) 229463, http://dx.doi.org/10.1016/j.jpowsour.2021.229463, URL: https://www.sciencedirect.com/science/article/pii/S037877532100015X.

[41] P. Buschel, T. Gunther, O. Kanoun, Distribution of relaxation times for effect identification and modeling of impedance spectra, in: 2014 IEEE International Instrumentation and Measurement Technology Conference, I2MTC Proceedings, IEEE, Montevideo, Uruguay, 2014, pp. 901–904, http://dx.doi.org/10.1109/I2MTC.2014.6860872, URL: http://ieeexplore.ieee.org/document/6860872/.

[42] J. Wainer, P. Fonseca, How to tune the RBF SVM hyperparameters? An empirical evaluation of 18 search algorithms, Artif. Intell. Rev. 54 (6) (2021) 4771–4797, http://dx.doi.org/10.1007/s10462-021-10011-5, URL: https://link.springer.com/article/10.1007/s10462-021-10011-5.

[43] S. Käbitz, J.B. Gerschler, M. Ecker, Y. Yurdagel, B. Emmermacher, D. André, T. Mitsch, D.U. Sauer, Cycle and calendar life study of a graphite|LiNi1/3Mn1/3Co1/3O2 Li-ion high energy system. Part a: Full cell characterization, J. Power Sources 239 (2013) 572–583, http://dx.doi.org/10.1016/j.jpowsour.2013.03.045, URL: https://www.sciencedirect.com/science/article/pii/S0378775313004369.

[44] G. Kucinskis, M. Bozorgchenani, M. Feinauer, M. Kasper, M. Wohlfahrt-Mehrens, T. Waldmann, Arrhenius plots for Li-ion battery ageing as a function of temperature, C-rate, and ageing state – An experimental study, J. Power Sources 549 (2022) 232129, http://dx.doi.org/10.1016/j.jpowsour.2022.232129, URL: https://www.sciencedirect.com/science/article/pii/S0378775322011065.

[45] S.S. Keerthi, C.-J. Lin, Asymptotic behaviors of support vector machines with Gaussian kernel, Neural Comput. 15 (7) (2003) 1667–1689, http://dx.doi.org/10.1162/089976603321891855.